Effects of geometric nonlinearity in an adhered microbeam for measuring the work of adhesion

Wenqiang Fang[a], Joyce Mok[a], Haneesh Kesari[a,]

[a]*School of Engineering, Brown University, Providence, RI-02906, USA*

Abstract

Design against adhesion in microelectromechanical devices is predicated on the ability to quantify this phenomenon in microsystems. Previous research related the work of adhesion for an adhered microbeam to the beam's unadhered length, and as such, interferometric techniques were developed to measure that length. We propose a new vibration-based technique that can be easily implemented with existing atomic force microscopy tools or similar metrology systems. To make such a technique feasible, we analyzed a model of the adhered microbeam using the nonlinear beam theory put forth by Woinowsky-Krieger. We found a new relation between the work of adhesion and the unadhered length; this relation is more accurate than the one by Mastrangelo redand Hsu (*J. Microelectromech S.*, **2**, 44-55. (doi:10.1109/84.232594)) which is commonly used. Then, we derived a closed-form approximate relationship between the microbeam's natural frequency and its unadhered length. Results obtained from this analytical formulation are in good agreement with numerical results from 3D nonlinear finite element analysis.

Keywords: micromechanics, adhesion, stiction, nonlinear beam theory

1. Introduction

Microelectromechanical systems (MEMS) technology has the capability of connecting digital electronics to the physical world through sensing, actuation or other mechanical means. Current MEMS technologies under research include pressure transducers, accelerometers, microactuators [1, 2], biomedical devices [3], optical components [4] and radio frequency (RF) MEMS switches [5]. However, a critical impediment to the full commercialization of MEMS devices is reliability.

Email address: haneesh_kesari@brown.edu (Haneesh Kesari)

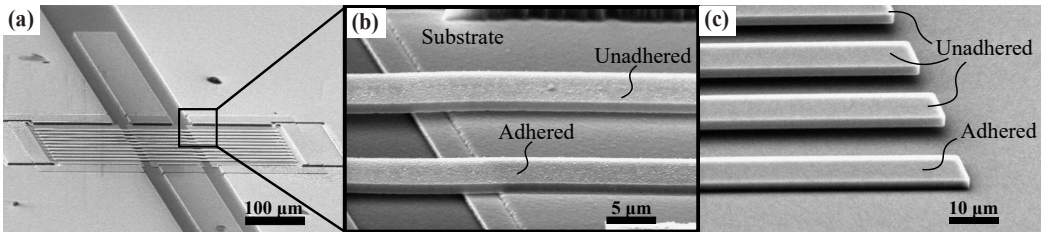

Figure 1: (a) Scanning electron micrograph of RF MEMS bridge composed of aluminum (with small additional percentage of silicon) and tantalum pentoxide dielectric coating on the substrate [6]. b) Close-up of adhered (front) and unadhered (rear) members of bridge [6]. (c) Array of cantilevered microbeams with the foremost beam adhered [7]

Stiction, the unintentional adhesion of compliant microstructure surfaces [8], is notorious for causing serious reliability concerns [9]. Stiction occurs because surface forces (e.g. capillary, electrostatic and van der Waals) dominate at submicron scales [10, 7]. When elastic restoring forces of structures are unable to overcome these strong adhesive forces, surfaces remain permanently adhered to each other and cause device failure [11] (see Fig. 1).

Stiction may occur at two stages in the life of a MEMS device: fabrication and in-use. Stiction failure during the fabrication stage is usually caused by capillary forces during the release process. Thus, it can be avoided through methods such as dry etching [12], super critical drying [13] and freeze drying [9]. In-use stiction is more difficult to prevent. Straightforward methods for preventing in-use stiction include the stiffening of structures [14] and increasing the gap size between the devices and substrates [15]. However, these two methods may be undesirable for device performance [16]. Other solutions have been reported such as the use of bumps [17], electric force induced vibration [18, 19, 20] and surface texturing [21]. The most promising results have come from research in anti-stiction [22] and self-assembled monolayer coatings [23]. Standardization of these techniques requires the ability to quantify stiction – measuring the work of adhesion w [1]and studying its dependence on parameters such as surface morphology, hydrogen termination [24] and environmental conditions [25].

[1]The work of adhesion w is defined as $w = \gamma_1 + \gamma_2 - \gamma_{12}$ where γ_1 and γ_2 are the energies needed to create new surfaces of each respective material and γ_{12} is the energy required to create a unit area of interface between the two surfaces [26]. In the case where the two materials are the same, γ_{12} is zero and the w reduces to $w = 2\gamma_1 = 2\gamma_2$. Other notations may simply refer to this case as $w = 2\gamma$ with w also called the interfacial surface energy [27]. In our formulation, we refer to w in the general sense, whereas in the work of Mastrangelo redand Hsu [28], the materials of

1.1. Measuring the work of adhesion using microbeam arrays

Previous work [29, 30] has related w to the unadhered length a (see Fig. 2red(c)) of the microbeam. This length a is a characteristic of the cantilever's geometry, mechanical properties of the cantilever's material, and w between the surfaces of the cantilever and substrate. Experiments could then be performed to measure a and calculate w.

Mastrangelo redand Hsu [29] developed an interferometric method for finding a through an array of cantilevers of increasing length, similar to that shown in Fig. 1(c). For this method, they fabricated an array of microbeams on a single chip through sacrificial etching with hydrofluoric acid. Microbeams of length greater than a would become adhered due to capillary forces during the drying process, while shorter microbeams would be unadhered. The shortest adhered microbeam with length closest to a could then be identified through a change in the interference pattern over the array. This technique has limitations that prevent its widespread application. First, it is required that a whole array of cantilevers be manufactured on a single chip such that the adherence is caused by capillary forces pulling the beams down to the substrate. The combinations of substrate and microbeam materials in such arrays are limited to what can be made on a single chip through such microfabrication techniques. If one desires to characterize adhesion between surface pairs that have been made of different materials, have undergone different surface treatments or have different small-scale geometric features, then multiple arrays must be manufactured. If one redwants to calculate statistics on the measurement of a, redthen even more arrays must be made. The resolution of each measurement also depends on the difference in length between each adjacent cantilever, and choice of what range of lengths of cantilevers to manufacture presupposes some knowledge of what the unadhered length a could be (knowledge which is not always available since that is the value that the experiment is meant to find).

redDe Boer and Michalske [30] performed similar experiments but redused long microbeams adhered over long attachment lengths. Instead of observing a change in the interference pattern over a whole array redof microbeams, a linescan over the top surface of redeach single beam was performed to acquire redthe vertical displacements over the redwhole length of that beam. From plots of the vertical displacementreds of the beam versus the length of the beam, a could redthen be found. redDe Boer and Michalske's method provides improvements

---

the beam and substrate are assumed to be the same so that $w = 2\gamma$.

over that of Mastrangelo redand Hsu's. For example, issues of the resolution of the measurement depending on the difference in lengths of adjacent cantilevers redare avoided. It is also not necessary redto make a full array of cantilevers. However, it does require a full linescan of the microbeam such that multiple data points must be processed to find a single experimental value of a. This data processing must then be repeated for multiple microbeams if one wanted to calculate statistics on the measured value of a.

1.2. Vibration based technique for measuring work of adhesion

Alternatively, we envision a vibration-based technique which we believe could give a highly accurate estimate of a from a single point measurement. The motivation for this idea is that vibration-based techniques of measurement are well established, are known to have high sensitivity and repeatability and are easy to use on a MEMS chip [31, 32]. This technique would be implementable on an atomic force microscope (AFM) or related surface metrology tools that involve mechanical contact between a cantilevered structure and a surface. We illustrate how this technique would work in Fig. 2(a)–(d).

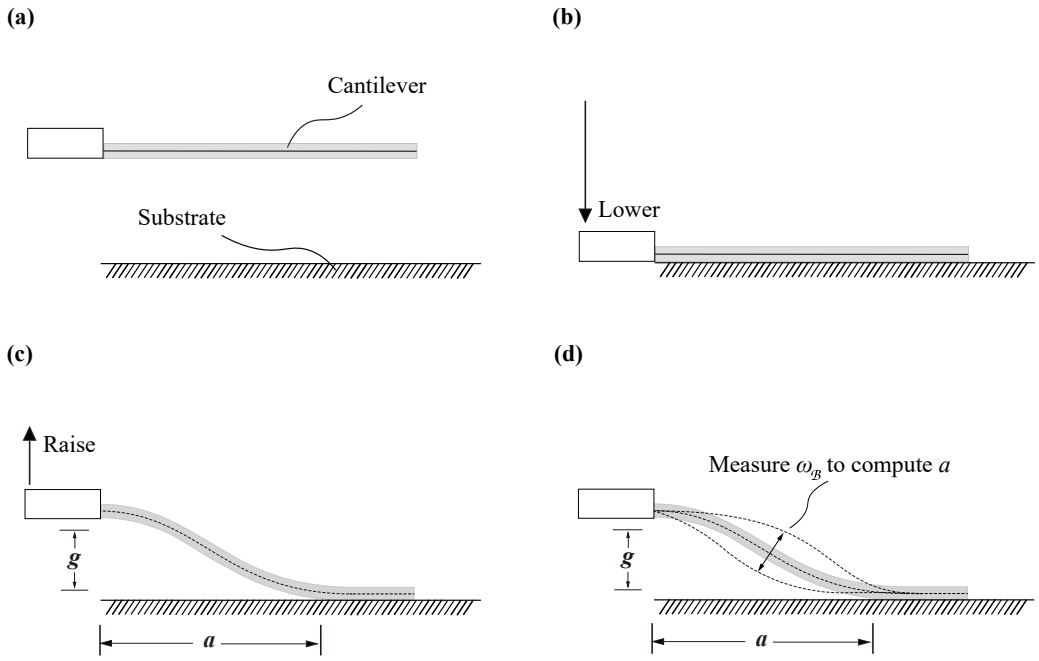

Figure 2: (a) Cantilever is positioned above the substrate. (b) The cantilever is brought down to the substrate until it has adhered. (c) The cantilever is brought up a fixed distance g. (d) The natural frequency $\omega_{\mathcal{B}}$ of the adhered configuration of the cantilever is measured to compute a.

In an AFM system, a commercially available tipless cantilever [33] or one that is specially manufactured [34] can be brought into contact with a surface and then lifted a distance g. With the cantilever in its adhered configuration, its natural frequency can redthen be found by measuring its thermal fluctuations; measurement of the natural frequency through thermal fluctuations is already implemented as part of a well-defined calibration method for AFM cantilevers [35, 36, 37, 38, 39]. Besides AFMs, there exist other examples of cantilever-based mechanical measurement systems being used in research [40, 41]. Thus, measuring the vibration of a microbeam is a feasible method to find a. However, as we detail below, no satisfactory formula connecting the fundamental natural frequency of the adhered microbeam $\omega_{\mathcal{B}}$ to a is currently available. Therefore, we derive such a formula in Section 33.2.

1.3. Justification for deriving a new relation between the unadhered length and natural frequency of the adhered microbeam

Study of the vibrations of structures is a well established subject. Closed-form expressions for the natural frequencies of a number of structural mechanics models can be found in standard textbooks on the subject. These structures include strings, bars, shafts and beams in 1D and membranes, plates and shells in 2D [42]. Due to the microbeam's high aspect ratio, several researchers have studied both the free and forced vibrations of microbeams using beam theories. For example, Tilmans *et al.* [43, 44, 45] studied the natural vibration of a free standing MEMS microbeam using a modified Euler-Bernoulli beam theory. In the original version of the Euler-Bernoulli theory, the structure only transmits bending moments and shear forces along its length, whereas in the modified theory used by Tilmans *et al.*, the structure additionally transmits a constant tensile force. redGhayesha *et al*.[46, 47, 48, 49, 50, 51] and Farokhi *et al.* [52, 53] studied redthe nonlinear dynamics of microbeams by considering the size effect. They obtained size-dependent frequency-response curves of both Euler-Bernoulli beams and Timoshenko beams through Galerkin and pseudo-arclength continuation techniques. Zhang redand Zhao [54] studied the forced vibration of an adhered MEMS microbeam. The forcing was applied through a time varying voltage between the microbeam and substrate, and the adhered beam was modeled using a nonlinear beam theory. In addition to the bending energy, the model included two additional terms in the elastic potential energy of the beam that the authors refer to as the "stretching energy" terms. They used Galerkin and Newton-Raphson numerical methods to solve the governing equations of their model. However, they provided neither a closed form expression for the adhered microbeam's fundamental natural frequency nor any theoretical analysis on the frequency's dependence on the problem parameters. Such a closed form expression is critical for determining a from $\omega_{\mathcal{B}}$. Consequently, the previous work of Zhang redand Zhao is not directly applicable to our proposed vibration based method for measuring $\omega_{\mathcal{B}}$.

Therefore, we derive a closed form expression relating a to $\omega_{\mathcal{B}}$ using nonlinear beam theory. We used the theory commonly called "extensible beam theory" to predict the microbeam's natural frequency. This theory is based off of the work of Woinowsky-Kreiger [55] who used it to study the effect of axial stress on the vibration of a simply supported beam. Thus, we will refer to it as Woinowsky-Kreiger theory.

Outline of paper. In Section 2, we review previous theory by Mastrangelo redand Hsu [29, 28] relating a to w of the microbeam. The full derivation of our formula

connecting a to $\omega_{\mathcal{B}}$ is presented in Section 3. Our predictions of the deformed configuration of the microbeam match nonlinear finite element analysis (FEA) results better than the configuration reported by Mastrangelo redand Hsu [28], which is currently widely used; these comparisons are shown in Section 44.1. In Section 44.2, we use our model to compute fundamental frequencies under different parameters and compare those values with nonlinear FEA results; errors were found to be less than or equal to 1% for a range of parameters representative of beam structures typically found in MEMS devices and AFM cantilevers.

2. Previous work connecting the unadhered length to the work of adhesion

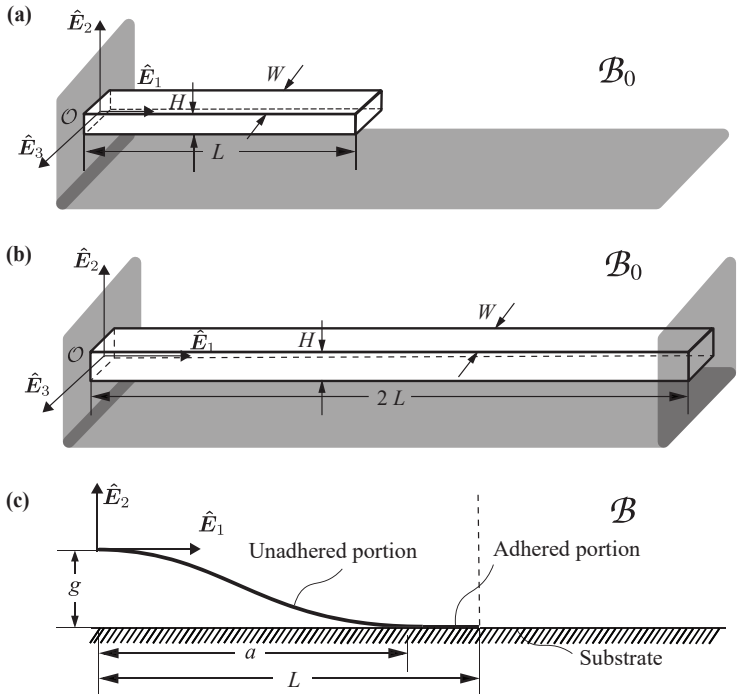

Figure 3: Schematic of the reference configuration, $\mathcal{B}_0$, (a) of a cantilevered microbeam and (b) of a fixed-fixed microbeam. (c) Schematic of a static, adhered configuration of a microbeam. This adhered configuration corresponds to both the cantilever and the left half of the fixed-fixed microbeam which is symmetric with the right. For elaboration on this point, see Section 22.2.

Mastrangelo redand Hsu [29, 56, 28] previously studied the adhered shapes of microbeams whose geometries are shown in Fig. 3.

2.1. Cantilevered microbeams

The microbeam shown in Fig. 3(a) is a cantilevered beam, as in, one of its ends is fixed while the other is free. This is the geometry of micromachined AFM probes (Fig. 2) and redthose of other cantilever-based metrology systems and is therefore relevant to our proposed vibration-based method for measuring w. Fig. 3 also shows the vectors $\hat{\boldsymbol{E}}_i$, $i = 1,\ 2,\ 3$, which form an orthonormal set of Cartesian basis vectors. The origin of the coordinate system, marked O, is located at the left fixed support of the microbeam. We refer to the unadhered, free-standing configuration of the microbeam (Fig. 3(a)) as the reference configuration $\mathcal{B}_0$. In its reference configuration, the cantilever is stress free[2] and occupies the cuboidal region $[0, L]\times[-H/2, H/2]\times[-W/2, W/2]$. That is, it is straight with length L and has a rectangular cross-section of width W and height H that is perpendicular to the $\hat{\boldsymbol{E}}_1$ direction. It is positioned parallel to the substrate at a distance g above it.

Mastrangelo redand Hsu and other researchers [58, 30, 59] have previously studied the mechanics of adhered microbeams using a configurational force balance approach. This approach was pioneered by Griffith [60]. The techniques of configurational force balance have since been greatly expanded [61] and have been applied to problems such as redthe adhesion of thin films, redthe peeling of lap joints and double torsion tests [62]. Per this perspective, a configuration is considered to be locally stable (metastable) if and only if infinitesimal perturbations around that configuration lead to an increase in the system's potential energy Π. For the adhered microbeam, this requirement implies that

$$\frac{\partial \Pi}{\partial A_a} = 0 \tag{2.1}$$

[2] In [56], Mastrangelo redand Hsu give the elastic potential energy of the fixed-fixed microbeam to be $\frac{512g^2EI}{5(2a)^3}\left[1 + \frac{T(2a)^2}{42EI} + \frac{256}{735}\left(\frac{g}{H}\right)^2\frac{a}{L}\right]$, where $T = WH\sigma_R$ is the axial residual tensile force and σ_R is the internal residual tensile stress. Such residual stresses generally arise as a consequence of the microfabrication processes used for manufacturing the microbeams [57]. However, such stresses are likely to be absent in the AFM microcantilevers that will be employed in our proposed, new experimental method (Fig. 2red(a)–(d). Thus, we ignore residual stresses in our current work. The expression for the elastic potential energy given in (2.8) was obtained by putting $\sigma_R = 0$ in the expression given by Mastrangelo redand Hsu in [56, 28]. Also, there is a difference of a factor of 1/2 between the two expressions. This is because the expression in (2.8) corresponds to only one half of the symmetric, fixed-fixed microbeam, whereas that given by Mastrangelo redand Hsu in [56, 28] corresponds to the full beam.

where A_a is the magnitude of the area over which the microbeam and the substrate are in contact. Generally, it is assumed that the contact region formed between the cantilever and the substrate is simply connected and its delamination front is straight and parallel to the $\hat{E}_3$ direction. Consequently, (2.1) is equivalent to the condition

$$\frac{\partial \Pi}{\partial a} = 0, \tag{2.2}$$

where a is the unadhered length of the microbeam (see Fig. 3(c)).

For the adhered microbeam, the total potential energy Π consists of two terms: the redadhesion energy $\Pi_{\mathcal{S}}$ and the elastic potential energy $\Pi_{\mathcal{E}}$. The redadhesion energy (see [29][3]) is generally taken to be

$$\Pi_{\mathcal{S}} = -w(L-a)W. \tag{2.3}$$

In [29], Mastrangelo redand Hsu used Euler-Bernoulli beam theory [63] to model the adhered microbeam. As such, the microbeam's elastic potential energy was taken to be

$$\Pi_{\mathcal{E}} = \int_0^a \frac{EI}{2}\left(\frac{\partial^2 U_2(X_1)}{\partial X_1^2}\right)^2 dX_1 \tag{2.4}$$

where E is the Young's modulus, I is the second moment of area of the microbeam's cross-section, X_1 is the Cartesian coordinate corresponding to the $\hat{\boldsymbol{E}}_1$ direction, and

$$U_2(X_1) = -g\left(\frac{X_1}{a}\right)^2\left(3 - 2\frac{X_1}{a}\right), \tag{2.5}$$

which is the the displacement of the microbeam's midsurface in the $\hat{\boldsymbol{E}}_2$ direction (Fig. 3(c)). By substituting (2.5) into (2.4), we find $\Pi_{\mathcal{E}}$ to be

$$\Pi_{\mathcal{E}} = \frac{6EIg^2}{a^3}. \tag{2.6}$$

Computing Π by summing the expressions for $\Pi_{\mathcal{E}}$ and $\Pi_{\mathcal{S}}$ given by (2.6) and (2.3), respectively, then substituting into (2.2), Mastrangelo redand Hsu found the relation between w and a to be

$$w = \frac{3EH^3g^2}{2a^4}. \tag{2.7}$$

[3] In this case, the authors of [29] followed the assumption that the two surfaces, substrate and beam, were of the same material; then, w is equivalent to 2γ.

2.2. Fixed-fixed microbeams

Mastrangelo redand Hsu [28] also studied the adhered microbeam in the fixed-fixed configuration shown in Fig. 3(b). These types of microbeams are found in RF MEMS capacitive switches (Fig. 1(a)). This geometry is not relevant to our proposed experimental method. Nonetheless, we still discuss it since our results apply to it.

In its reference configuration, the cantilever microbeam that we use for our derivations is equivalent to the reference configurations of both the left and right halves of the fixed-fixed microbeam. Following Mastrangelo redand Hsu [28], we assume that the fixed-fixed beam is symmetric about its midsection even in its adhered configuration. Owing to this assumpton and the manner in which our cantilever microbeam comes into contact with the substrate (Fig. 2(a)–(d)), even when adhered, the cantilever microbeam we study is equivalent to both the left and right halves of the fixed-fixed microbeam.

Mastrangelo redand Hsu analyzed the fixed-fixed microbeam using a nonlinear beam theory. Per that theory, the elastic potential energy of half of the fixed-fixed microbeam is[2]

$$\Pi_{\mathcal{E}} = \frac{256g^2EI}{5(2a)^3}\left[1 + \frac{256}{735}\left(\frac{g}{H}\right)^2\frac{a}{L}\right]. \tag{2.8}$$

Computing Π by summing $\Pi_{\mathcal{E}}$ given by (2.8) with $\Pi_{\mathcal{S}}$ given by (2.3), then substituting into (2.2), we find that for the fixed-fixed beam model given in [28], w and a are related by[4]

$$w = \frac{8Eg^2H^3}{5a^4}\left[1 + \frac{512}{2205}\left(\frac{g}{H}\right)^2\frac{a}{L}\right]. \tag{2.9}$$

In the next section, we present a new, more accurate formula relating w to a.

3. Nonlinear model for the adhered microbeam

We model the adhered microbeam using Woinowsky-Kreiger beam theory [55]red , which is a geometricredally nonlinear beam theory. We derive the equations

[4] Mastrangelo redand Hsu [28] give the relation between w and a as $w = \frac{8Eg^2H^3}{5a^4}\left[1 + \frac{256}{2205}\left(\frac{g}{H}\right)^2\right]$. We believe that the numerical factor 256/2205 in this equation is an error. Based on the expressions for the adhesion and elastic potential energies given in (2.3) and (2.8), respectively, the numerical factor should instead be 512/2205 (c.f. (2.9)).

governing its motion using Lagrangian mechanics. The potential and kinetic energies of the microbeam as per Woinowsky-Kreiger theory are

$$\Pi_{\mathcal{E}} = \int_0^a \left[\frac{EI}{2} \left(\frac{\partial^2 U_2}{\partial X_1^2} \right)^2 + \frac{EA}{2} \left(\frac{\partial U_1}{\partial X_1} + \frac{1}{2} \left(\frac{\partial U_2}{\partial X_1} \right)^2 \right)^2 \right] dX_1, \tag{3.1a}$$

$$\mathcal{T} = \frac{\rho A}{2} \int_0^a \left[\left(\frac{\partial U_1}{\partial t} \right)^2 + \left(\frac{\partial U_2}{\partial t} \right)^2 \right] dX_1, \tag{3.1b}$$

respectively, where $U_1(X_1, t)$ and $U_2(X_1, t)$ are the displacements of the material point X_1 on the beam's centroidal axis at time t in the $\hat{\boldsymbol{E}}_1$ and $\hat{\boldsymbol{E}}_2$ directions, respectively. Here, A is the area of the beam's cross-section and ρ is the density of the material of the beam.

We introduce the following non-dimensional variables: $\hat{a} := a/H$, $\hat{g} := g/H$, $\hat{w} := w/(EH)$, $\xi := X_1/a$, $\zeta := U_1/H$, $\eta := U_2/H$, $\omega_0 := \sqrt{EI/\rho A r e d a^4}$, $\tau := t\omega_0$, $\hat{\Pi}_{\mathcal{E}} := 24a^3\Pi_{\mathcal{E}}/(H^5 WE)$, and $\hat{\mathcal{T}} := 24a^3\mathcal{T}/(H^5 WE)$. In terms of these variables (3.1a)–(3.1b) read as

$$\hat{\Pi}_{\mathcal{E}} = \int_0^1 \left[\left(\frac{\partial^2 \eta}{\partial \xi^2} \right)^2 + 12 \left(\hat{a} \frac{\partial \zeta}{\partial \xi} + \frac{1}{2} \left(\frac{\partial \eta}{\partial \xi} \right)^2 \right)^2 \right] d\xi, \tag{3.2a}$$

$$\hat{\mathcal{T}} = \int_0^1 \left[\left(\frac{\partial \zeta}{\partial \tau} \right)^2 + \left(\frac{\partial \eta}{\partial \tau} \right)^2 \right] d\xi. \tag{3.2b}$$

Applying Hamilton's principle and using the expressions for the potential and kinetic energies given in (3.2a) and (3.2b), the Euler-Lagrange equations governing the motion of the microbeam come out to be

$$\frac{\partial^2 \zeta}{\partial \tau^2} - 12\hat{a} \frac{\partial}{\partial \xi} \left(\hat{a} \frac{\partial \zeta}{\partial \xi} + \frac{1}{2} \left(\frac{\partial \eta}{\partial \xi} \right)^2 \right) = 0, \tag{3.3a}$$

$$\frac{\partial^2 \eta}{\partial \tau^2} + \frac{\partial^4 \eta}{\partial \xi^4} - 12 \frac{\partial}{\partial \xi} \left[\left(\hat{a} \frac{\partial \zeta}{\partial \xi} + \frac{1}{2} \left(\frac{\partial \eta}{\partial \xi} \right)^2 \right) \frac{\partial \eta}{\partial \xi} \right] = 0. \tag{3.3b}$$

The equations (3.3a)–(3.3b) are subject to the boundary conditions[5]

$$\zeta = 0, \quad \eta = 0, \quad \frac{\partial \eta}{\partial \xi} = 0, \quad \text{at } \xi = 0, \ \forall \tau, \tag{3.4a}$$

$$\zeta = 0, \quad \eta = -\hat{g}, \quad \frac{\partial \eta}{\partial \xi} = 0, \quad \text{at } \xi = 1, \ \forall \tau. \tag{3.4b}$$

It is challenging to derive a general, closed form solution to the nonlinear partial differential equations (PDEs) (3.3a)–(3.3b). However, recall that we do not need to know the general dynamical behavior of the adhered microbeam. We are only interested in the vibratory motion that the microbeam may execute about a static, adhered configuration (see Fig. 4), which is relevant within the context of our proposed experimental method. Therefore, we attempt to solve (3.3a)–(3.3b) approximately by making the ansatz that the vibratory solution that we seek admits the asymptotic expansion

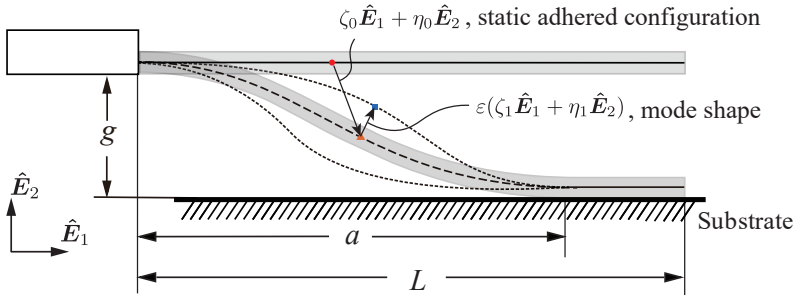

Figure 4: Schematic of the static configuration and the mode shape of the adhered, vibrating microbeam.

red

$$\zeta(\xi,\tau) = \zeta_0(\xi) + \varepsilon\zeta_1(\xi)\cos(\hat{\omega}_{\mathcal{B}}\tau) + O(\varepsilon^3), \tag{3.5a}$$

$$\eta(\xi,\tau) = \eta_0(\xi) + \varepsilon\eta_1(\xi)\cos(\hat{\omega}_{\mathcal{B}}\tau) + O(\varepsilon^3), \tag{3.5b}$$

where red$\zeta_0(\xi)$ and red$\eta_0(\xi)$ describe the static shape of the adhered microbeam assumed in the absence of any dynamical motion, and red$\varepsilon\zeta_1(\xi)\cos(\hat{\omega}_{\mathcal{B}}\tau)$ and

[5] Due to manner in which the microbeam is brought into contact with the substrate (see Figs. 2 (c)–(d)) there are no displacements in the microbeam until it comes into contact with the substrate. After the microbeam and the substrate make contact, we assume that there is no slippage, i.e. $\zeta = 0$, in the adhered portion of the microbeam as its base moves to a height g above the substrate (see Figs. 2red(b)–(d)). Recall that once the microbeam's base reaches a height g, it is held fixed at that height. We assume that after the microbeam's base reaches the height g, the unadhered length a also remains fixed irrespective of any dynamical behavior that the microbeam may display. Finally, we assume that there is no slippage in the adhered portion of the microbeam after the microbeam's base reaches the height g. The boundary condition $\zeta = 0$ at $\xi = 1$ is a consequence of these assumptions.

red$\varepsilon\eta_1(\xi)\cos(\hat{\omega}_{\mathcal{B}}\tau)$ are the leading order terms relating to the microbeam's vibratory motion. The parameter ε is the non-dimensional amplitude of the microbeam's vibratory motion, and $\hat{\omega}_{\mathcal{B}} = \omega_{\mathcal{B}}/\omega_0$ is the non-dimensional fundamental, natural frequency of the adhered microbeam. The symbol $O(\varepsilon^3)$ in (3.5b) and (3.5a) denotes all terms in the solution that vanish at a rate that is faster than or equal to ε^3 as $\varepsilon \to 0$. Since vibratory motion is by definition of infinitesimal magnitude, we limit our analysis to the special case of $\varepsilon \to 0$.

Substituting the asymptotic forms red(3.5a)–(3.5b) into the nonlinear PDEs (3.3a)–(3.3b) and the boundary conditions (3.4a)–(3.4b) and then integrating the resulting equations with respect to τ for 0 to $2\pi/\hat{\omega}_{\mathcal{B}}$, we find that red$\zeta_0$ and redη_0 satisfy the nonlinear ordinary differential equations

$$\frac{d\epsilon_0^2}{d\xi} = 0, \tag{3.6a}$$

$$\frac{d^4\eta_0}{d\xi^4} - 4\epsilon_0^2\frac{d^2\eta_0}{d\xi^2} = 0, \tag{3.6b}$$

where ϵ_0^2 *red*: $= 3\hat{a}(d\zeta_0/d\xi) + 3\left(\partial\eta_0/\partial\xi\right)^2/2$, that are subject to the boundary conditions

$$\zeta_0 = 0, \quad \eta_0 = 0, \quad \frac{d\eta_0}{d\xi} = 0, \quad \text{at } \xi = 0, \tag{3.7a}$$

$$\zeta_0 = 0, \quad \eta_0 = -\hat{g}, \quad \frac{d\eta_0}{d\xi} = 0, \quad \text{at } \xi = 1. \tag{3.7b}$$

Solving (3.6a)–(3.7b), we get

$$\zeta_0(\xi) = \frac{\epsilon_0^2}{6\hat{a}}\left(\frac{3(1-2\xi)\sinh(2\epsilon_0) + \sinh(2\epsilon_0 - 4\xi\epsilon_0) - 8\cosh(\epsilon_0)\sinh(\epsilon_0 - 2\xi\epsilon_0)}{4\epsilon_0 - 3\sinh(2\epsilon_0) + 2\epsilon_0\cosh(2\epsilon_0)}\right), \tag{3.8a}$$

$$\eta_0(\xi) = \hat{g}\frac{2\xi\epsilon_0\cosh\epsilon_0 + \sinh(\epsilon_0 - 2\xi\epsilon_0) - \sinh\epsilon_0}{2\sinh\epsilon_0 - 2\epsilon_0\cosh\epsilon_0}, \tag{3.8b}$$

where ϵ_0 is related to $\hat{g}$ through the equation

$$\hat{g}^2 = \frac{8\epsilon_0(\sinh\epsilon_0 - \epsilon_0\cosh\epsilon_0)^2}{6\epsilon_0(\cosh 2\epsilon_0 + 2) - 9\sinh 2\epsilon_0}. \tag{3.9}$$

Unfortunately, we could not invert (3.9) to get ϵ_0 as a function of $\hat{g}$. However, we found that

$$\epsilon_0 \approx \frac{3\hat{g}}{2}\sqrt{\frac{3\hat{g}\left[4\hat{g} - \sqrt{5}\sinh\left(6\hat{g}/\sqrt{5}\right) + 2\hat{g}\cosh\left(6\hat{g}/\sqrt{5}\right)\right]}{2\left[\sqrt{5}\sinh\left(3\hat{g}/\sqrt{5}\right) - 3\hat{g}\cosh\left(3\hat{g}/\sqrt{5}\right)\right]^2}}. \tag{3.10}$$

redDetails of how this approximation was obtained can be found in Appendix Appendix A. The quality of this approximation for ϵ_0 can be ascertained from Fig. 5, in which the approximate values of ϵ_0 given by (3.10) are compared with the exact values of ϵ_0 that we obtained by numerically solving (3.9).

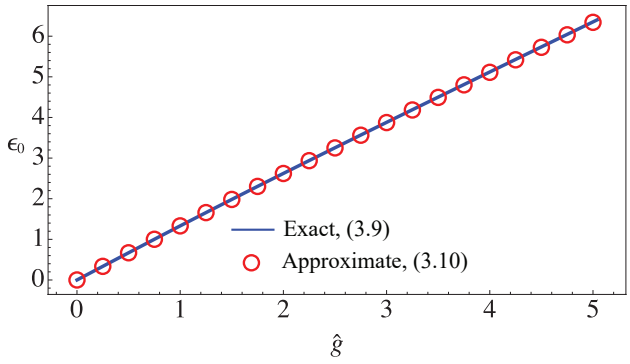

Figure 5: A plot of the values of ϵ_0 calculated through the approximate relation (3.10) and calculated through numerically solving the exact relation (3.9). The relative error between the two equations at $\hat{g} = 5$ is approximately 0.174%.

3.1. A new relation between the unadhered length and the work of adhesion

Substituting redζ_0 and redη_0 given by red(3.8a)–(3.8b) into red(3.5a)–(3.5b) and then substituting the resulting asymptotic expansions for redζ and redη into (3.2a), we get

$$\hat{\Pi}_{\mathcal{E}}(\tau) = \langle \hat{\Pi}_{\mathcal{E}} \rangle + 2\varepsilon \cos(\hat{\omega}_{\mathcal{B}}\tau) \int_0^1 \left[\frac{d^2\eta_0}{d\xi^2}\frac{d^2\eta_1}{d\xi^2} + 4\epsilon_0^2 \left(\hat{a}\frac{d\zeta_1}{d\xi} + \frac{d\eta_0}{d\xi}\frac{d\eta_1}{d\xi} \right) \right] d\xi$$
$$+ \varepsilon^2 \cos^2(\hat{\omega}_{\mathcal{B}}\tau) \int_0^1 \left[\left(\frac{d^2\eta_1}{d\xi^2} \right)^2 + 12 \left(\hat{a}\frac{d\zeta_1}{d\xi} + \frac{d\eta_0}{d\xi}\frac{d\eta_1}{d\xi} \right)^2 + 4\epsilon_0^2 \left(\frac{d\eta_1}{d\xi} \right)^2 \right] d\xi + o(\varepsilon^2), \tag{3.11}$$

where

$$\langle \hat{\Pi}_{\mathcal{E}} \rangle = \frac{3\hat{g}^4\epsilon_0^2(4\epsilon_0 - 3\sinh 2\epsilon_0 + 2\epsilon_0 \cosh 2\epsilon_0)^2}{16(\sinh\epsilon_0 - \epsilon_0\cosh\epsilon_0)^4} - \frac{2\hat{g}^2\epsilon_0^3(\epsilon_0 - \sinh\epsilon_0\cosh\epsilon_0)}{(\sinh\epsilon_0 - \epsilon_0\cosh\epsilon_0)^2} \tag{3.12}$$

is a constant with respect to time. We refer to $\langle \hat{\Pi}_{\mathcal{E}} \rangle$ as the (non-dimensional) static, potential energy of the adhered microbeam.

The dimensional, elastic potential energy of the adhered microbeam, $\Pi_{\mathcal{E}}$, can be obtained by multiplying $\hat{\Pi}_{\mathcal{E}}(\tau)$ given by (3.11) by the factor $H^5WE/(24a^3)$. Combining the thus obtained $\Pi_{\mathcal{E}}$ with the redadhesion energy $\Pi_{\mathcal{S}}$ given by (2.3) to get Π, substituting that result into the configurational force balance equation (2.2), then taking the limit $\varepsilon \to 0$, we get

$$w = \frac{EH^5\langle\hat{\Pi}_{\mathcal{E}}\rangle}{8a^4}. \tag{3.13}$$

Note that $\langle\hat{\Pi}_{\mathcal{E}}\rangle$ only depends on $\hat{g}$. Thus, knowing a, an approximate value for w can be calculated using (3.13).

3.2. Relating the fundamental, natural frequency of an adhered microbeam to its unadhered length

We solve for $\omega_{\mathcal{B}}$ by equating the maximum of the absolute value of the difference in the adhered beam's kinetic energy between any two times instances to the corresponding maximum difference in its potential energy. This idea, based on the principle of energy conservation in elastic structures, is very similar to what is termed Rayleigh's energy method [64] in structural dynamics.

Substituting the functions redζ_0 and redη_0 given by red(3.8a)–(3.8b) into red(3.5a)–(3.5b), substituting the resulting asymptotic expansions into (3.2a)–(3.2b), evaluating the integrals in the resulting equations and simplifying, we get the maximum changes in the non-dimensional potential and kinetic energies to be

$$\Delta_{\max}[\hat{\Pi}_{\mathcal{E}}] = \varepsilon^2 \int_0^1 \left[\left(\frac{d^2\eta_1}{d\xi^2}\right)^2 + 12\left(\hat{a}\frac{d\zeta_1}{d\xi} + \frac{d\eta_0}{d\xi}\frac{d\eta_1}{d\xi}\right)^2 + 4\epsilon_0^2\left(\frac{d\eta_1}{d\xi}\right)^2\right] d\xi + O(\varepsilon^3), \tag{3.14a}$$

$$\Delta_{\max}[\hat{\mathcal{T}}] = \varepsilon^2\hat{\omega}_{\mathcal{B}}^2 red \int_0^1 \left(\zeta_1^2 + \eta_1^2\right) d\xi + O(\varepsilon^4). \tag{3.14b}$$

Equating $\Delta_{\max}[\hat{\Pi}_{\mathcal{E}}]$ and $\Delta_{\max}[\hat{\mathcal{T}}]$ given by (3.14a) and (3.14b), dividing both sides of the resulting equation by ε^2, and taking the limit $\varepsilon \to 0$, we get that

$$\hat{\omega}_{\mathcal{B}}^2 = \frac{\int_0^1 \left[\left(\frac{d^2\eta_1}{d\xi^2}\right)^2 + 12\left(\hat{a}\frac{d\zeta_1}{d\xi} + \frac{d\eta_0}{d\xi}\frac{d\eta_1}{d\xi}\right)^2 + 4\epsilon_0^2\left(\frac{d\eta_1}{d\xi}\right)^2\right] d\xi}{red\int_0^1 \left(\zeta_1^2 + \eta_1^2\right) d\xi}. \tag{3.15}$$

Equations governing redζ_1 and redη_1 can be derived using a procedure similar to that employed for deriving the governing equations (3.6a)–(3.6b) for redζ_0

and redη_0. However, we were unable to solve those equations analytically. Consequently, we derive an approximate expression for ω_B by making a reasonable choice for redζ_1 and redη_1 in (3.15). This step is similar to the process of choosing an approximate mode shape in Rayleigh's method.

Considering the boundary conditions (3.4a)–(3.4b), a reasonable choice for η_1 is the fundamental mode shape of a straight fixed-fixed beam, which can be described as

$$\eta_1(\xi) = (\cosh b\xi - \cos b\xi) - \lambda(\sinh b\xi - \sin b\xi) \tag{3.16}$$

where

$$\lambda = (\cosh b - \cos b)/(\sinh b - \sin b),$$

and b, approximately equal to 4.730, is the first non-trivial root of

$$\cos(b)\cosh(b) = 1.$$

It can be shown that when the chosen redζ_1 and redη_1 are only approximate, i.e., they do not exactly satisfy (3.3a)–(3.3b), then the corresponding estimate for $\omega_{\mathcal{B}}$ is an upperbound. Thus, we should choose ζ_1 to make the numerator of the expression on the right hand side of (3.15) as small as possible and denominator as large as possible. In light of this knowledge, a good choice for ζ_1 is

$$\zeta_1(\chi) = -\frac{1}{\hat{a}}\int_0^{\chi} \frac{d\eta_0}{d\xi}\frac{d\eta_1}{d\xi}\, d\xi, \tag{3.17}$$

where η_0 and η_1 are, respectively, given by (3.8b) and (3.16). This is because, for this choice of ζ_1, the second term in the numerator of (3.15) vanishes. Also, the expression for ζ_1 given by (3.17) satisfies the essential boundary conditions stipulated by (3.4a)–(3.4b).

Substituting the approximate redζ_1 and redη_1 given by (3.16) and (3.17) into (3.15) and simplifying we get that

$$\omega_{\mathcal{B}} = b^2\omega_0\left[1 + c(\epsilon_0)\hat{g}^2\right]^{1/2}, \tag{3.18}$$

where $\omega_0 := \sqrt{EI/\rho Areda^4}$ and

$$c(\epsilon_0) = c_0\epsilon_0\frac{\epsilon_0(\cosh 2\epsilon_0 + 2) - 3\sinh\epsilon_0\cosh\epsilon_0}{3(\epsilon_0\cosh\epsilon_0 - \sinh\epsilon_0)^2}, \tag{3.19}$$

in which the numerical constant $c_0 \approx 0.22$. Again, the exact relation between ϵ_0 and $\hat{g}$ was given by (3.9). redAfter integrating the term $\int_0^1 \eta_1^2 d\xi$ in the denominator

of (3.15), the term becomes unity. In arriving at (3.18), we redthen ignored the term $\int_0^1 \zeta_1^2 d\xi$ in the denominator in (3.15). This is because in (3.15) the term $\int_0^1 \zeta_1^2 d\xi$ is being added to unity, and $\int_0^1 \zeta_1^2 d\xi$ is very small compared to unity; since $\int_0^1 \zeta_1^2 d\xi \approx 0.87(\hat{g}/\hat{a})^2 + O((\hat{g}/\hat{a})^4)$, and for typical microbeam structures, $\hat{g}/\hat{a} << 1$ (see Figure 7 for typical ranges of $\hat{g}$ and $\hat{a}$).

4. Discussion

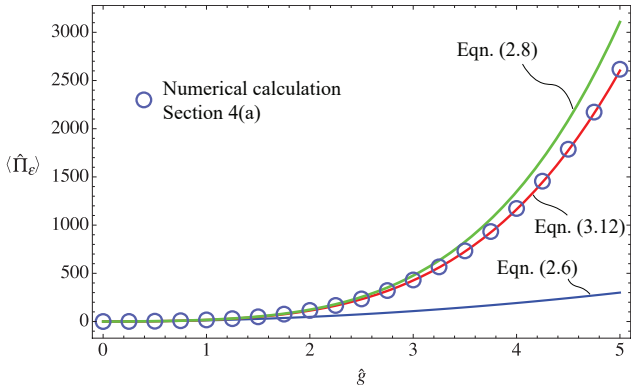

Figure 6: Elastic strain energy as a function of $\hat{g}$ as predicted by (2.6), (2.8), and (3.12) and numerical calculations. The numerical calculation results shown correspond to the parameter values $\hat{a} = 50$, $\hat{W} = 10$, and $\nu = 0.22$. The details of the numerical calculation are described in Section 44.1.

4.1. Comparison of the static elastic potential energy given by (3.12) *with numerical results*

In Figure 6, we compare a numerically computed $\langle\hat{\Pi}_\mathcal{E}\rangle$ against that computed from (3.12). We also show the elastic potential energy values given by equations (2.6) and (2.8), which we discussed in Section 2. The $\langle\hat{\Pi}_\mathcal{E}\rangle$ values given by (3.12) match the numerical calculation results much better than the elastic potential energy values given by either (2.6) or (2.8). The details of the calculations are given below.

We numerically computed the static elastic potential energy $\langle\hat{\Pi}_\mathcal{E}\rangle$ by solving a finite deformation continuum mechanics model of the adhered microbeam using nonlinear finite element procedures. The geometry of the numerical microbeam model was three dimensional and was the same as that shown in Fig. 3(a). We

assumed hyperelastic material behavior. Specifically, we assumed a compressible, neo-Hookean material model in which

$$\boldsymbol{S} = \lambda_0 \ln J \, \boldsymbol{C}^{-1} + \mu_0 \left(\boldsymbol{I} - \boldsymbol{C}^{-1} \right), \tag{4.1}$$

where $\boldsymbol{S}$ is the second Piola-Kirchhoff stress tensor, $\boldsymbol{C}$ is the right Cauchy-Green deformation tensor, J is the Jacobian determinant, $\boldsymbol{I}$ is the identity tensor, the parameters λ_0 and μ_0 are the Lamé constants, and $(\cdot)^{-1}$ is the inverse operator.

The right Cauchy-Green deformation tensor and the Jacobian determinant are defined as

$$\boldsymbol{C} := \boldsymbol{F}^{\mathsf{T}} \boldsymbol{F}, \tag{4.2}$$

$$J := \det(\boldsymbol{F}), \tag{4.3}$$

where

$$\boldsymbol{F} := \mathrm{Grad}(\boldsymbol{U}) \tag{4.4}$$

is the deformation gradient, $\det(\cdot)$ is the determinant operator, $\boldsymbol{U} := \sum_{i=1}^{3} U_i \hat{\boldsymbol{E}}_i$ is the displacement vector, $\mathrm{Grad}(\cdot)$ is the material gradient operator and $(\cdot)^{\mathsf{T}}$ is the transpose operator. The static, adhered configuration of the microbeam was obtained by solving the Cauchy momentum equation

$$\mathrm{Div}(\boldsymbol{F}\boldsymbol{S}) = 0, \tag{4.5}$$

on $\mathcal{B}_0$, where $\mathrm{Div}(\cdot)$ is the material divergence operator subject to the following boundary conditions: the displacements everywhere on the left face of the microbeam were fixed to be $(U_1, U_2, U_3) = (0, 0, 0)$, while that on the right face were everywhere fixed to be $(U_1, U_2, U_3) = (0, -g, 0)$.

The governing equations (4.1)–(4.5) were discretized using standard finite element procedures to obtain a system of nonlinear algebraic equations [65]. We used eight-node linear brick elements in the finite element mesh. The system of nonlinear algebraic equations were solved using the Newton-Raphson iterative procedure.

From the numerical solution, the static, elastic potential energy, $\langle \hat{\Pi}_{\mathcal{E}} \rangle$, of the adhered microbeam was computed as

$$\int_{\mathcal{B}_0} \frac{1}{2} \lambda_0 (\ln J)^2 - \mu_0 \ln J + \frac{1}{2} \mu_0 \left(\mathrm{tr}(\boldsymbol{C}) - 3 \right) \, d\Omega,$$

where $d\Omega$ is an infinitesimal volume element belonging to $\mathcal{B}_0$.

4.2. Comparison of the fundamental natural frequency $\omega_{\mathcal{B}}$ given by (3.18) *with numerical results*

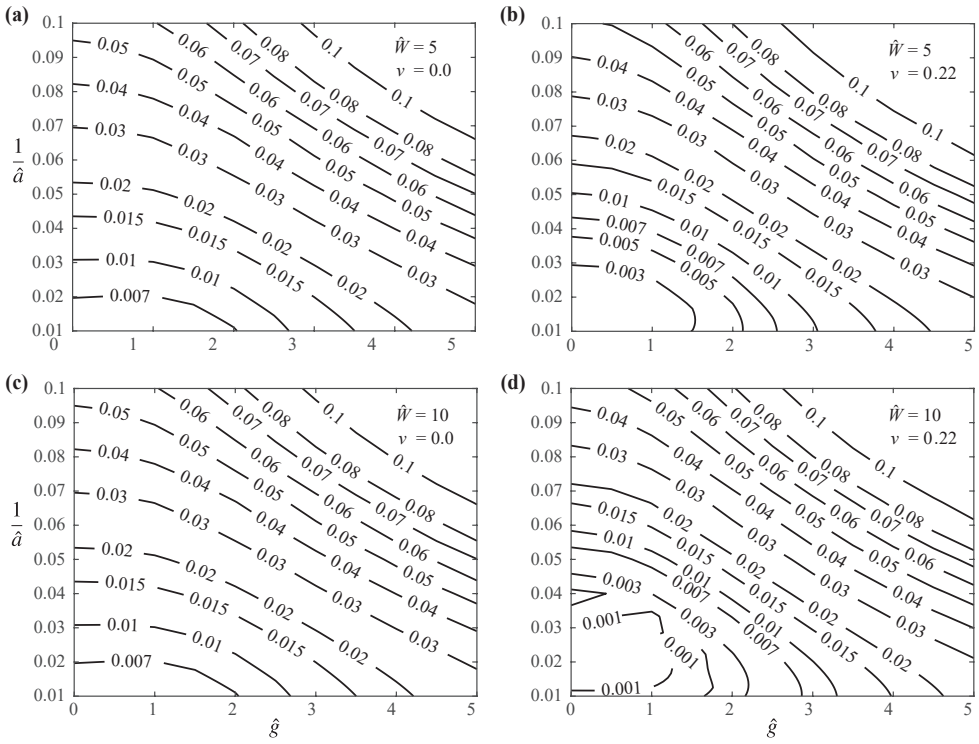

Figure 7: The relative percentage errors between numerical calculation results and analytical predictions for the fundamental, natural frequency, $\omega_{\mathcal{B}}$, of an adhered microbeam. See Section 44.2 for details of the numerical calculations.

We also compared the value of $\omega_{\mathcal{B}}$ given by (3.18) with numerical results. Figure 7 shows that the relative error between the analytical results and numerical calculation for $\omega_{\mathcal{B}}$ is proportional to $\hat{g}$ and inversely proportional to $\hat{a}$. Figure 7(b) shows that the difference between the analytical and numerical calculation for beams with width $\hat{W} = 5$ and Poisson's ratio $\nu = 0.22$ is less than 1% when $\hat{g} < 2.5$ and $1/\hat{a} < 0.025$, with other cases having similar error contours. Since the dimensions of structures in micromechanical devices are typically below these limits, we can conclude that (3.18) accurately represents the dependence of $\omega_{\mathcal{B}}$ on the system parameters. We detail the numerical calculations below.

Let $\bar{\boldsymbol{U}} : \mathcal{B}_0 \to \mathbb{R}^3$ be the displacement field corresponding to the microbeam's static, adhered configuration $\mathcal{B}$. This configuration is shown schematically in

Fig. 4. We discussed the method for numerically computing $\bar{\boldsymbol{U}}$ in Section 44.1. Similarly, the quantities $\bar{\boldsymbol{S}}$, $\bar{\boldsymbol{F}}$, $\bar{J}$, $\bar{\boldsymbol{C}}$, and $\bar{\boldsymbol{C}}^{-1}$ are the second Piola-Kirchhoff stress tensor, the deformation gradient, the Jacobian determinant, the right Cauchy-Green deformation tensor and its inverse corresponding to the static adhered configuration, respectively. We assume that the microbeam executes a vibratory motion with time varying displacements of the form $\Delta\boldsymbol{U}\cos(\omega_{\mathcal{B}}t)$ about the $\mathcal{B}$ configuration, such that $\boldsymbol{U} = \bar{\boldsymbol{U}} + \Delta\boldsymbol{U}\cos(\omega_{\mathcal{B}}t)$.

This vibratory motion leads to oscillations of the form $\Delta\boldsymbol{F}\cos(\omega_{\mathcal{B}}t)$ in $\boldsymbol{F}$, such that $\boldsymbol{F} = \bar{\boldsymbol{F}} + \Delta\boldsymbol{F}\cos(\omega_{\mathcal{B}}t)$. It follows from (4.4) that

$$\Delta\boldsymbol{F} = \mathrm{Grad}\,(\Delta\boldsymbol{U})\,. \tag{4.6}$$

Using (4.1)–(4.4), it can be shown that the second Piola-Kirchhoff stress would vary as

$$\boldsymbol{S} = \bar{\boldsymbol{S}} + \Delta\bar{\boldsymbol{S}}\cos(\omega_{\mathcal{B}}t) + o(\|\Delta\boldsymbol{F}\|), \tag{4.7}$$

where $\|\Delta\boldsymbol{F}\|$ denotes the norm of $\Delta\boldsymbol{F}$ and $\Delta\bar{\boldsymbol{S}}$ is related to $\Delta\boldsymbol{U}$ as

$$\Delta\bar{\boldsymbol{S}} = \bar{\mathbb{C}} : \frac{1}{2}\left(\bar{\boldsymbol{F}}^{\mathsf{T}}\mathrm{Grad}\,(\Delta\boldsymbol{U}) + \mathrm{Grad}\,(\Delta\boldsymbol{U})^{\mathsf{T}}\,\bar{\boldsymbol{F}}\right), \tag{4.8}$$

where the fourth order tensor $\bar{\mathbb{C}}$ is the material elasticity tensor, and the symbol ":" denotes double contraction.

For the constitutive law (4.1),

$$\bar{\mathbb{C}}_{IJKL} = \lambda_0\bar{C}^{-1}_{IJ}\bar{C}^{-1}_{KL} + (\mu_0 - \lambda_0\ln\bar{J})\left(\bar{C}^{-1}_{IK}\bar{C}^{-1}_{JL} + \bar{C}^{-1}_{IL}\bar{C}^{-1}_{KJ}\right),$$

where $\bar{\mathbb{C}}_{IJKL}$ and C^{-1}_{KJ} are the Cartesian components of the tensors $\bar{\mathbb{C}}$ and $\bar{\boldsymbol{C}}^{-1}$, respectively. Noting that $\mathrm{Div}(\bar{\boldsymbol{F}}\bar{\boldsymbol{S}}) = 0$, it follows from (4.5) that as $\|\Delta\boldsymbol{F}\| \to 0$ the displacement field $\Delta\boldsymbol{U}$ satisfies the equation

$$\mathrm{Div}\left(\bar{\boldsymbol{F}}\Delta\bar{\boldsymbol{S}} + \Delta\boldsymbol{F}\bar{\boldsymbol{S}}\right) = -\rho\omega^2_{\mathcal{B}}\Delta\boldsymbol{U}, \tag{4.9}$$

where ρ is the density of the material composing the microbeam. The boundary conditions on $\boldsymbol{U}$ stipulate that as $\Delta\boldsymbol{U}$ vanish on both ends of the microbeam.

Equation (4.9) is a linear partial differential equation in $\Delta\boldsymbol{U}$. We discretized (4.9) using standard, finite element procedures to get a linear, matrix-vector equation. However, in that matrix-vector equation, $\omega_{\mathcal{B}}$ was still an unknown. We therefore took it to be the smallest value for which the discretized form of (4.9) admitted a non trivial solution. Thus, the discrtetized form of (4.9) defined a standard

eigenvalue problem in linear algebra. We solved the eigenvalue problem using Lanczos' numerical method to get $\omega_{\mathcal{B}}$. In our finite element procedures, we used the same finite elements that we used for computing the static, adhered solution $\bar{\boldsymbol{U}}$. The number of elements varied from 2.5×10^4 (for $\hat{W} = 5$ and $\hat{a} = 10$) to 5×10^5 (for $\hat{W} = 10$ and $\hat{a} = 100$).

4.3. Asymptotic behavior of the w–a equation (3.13)

As $\hat{g} \to 0$, the displacements and displacement gradients become vanishingly small and in Woinowsky-Krieger theory reduces to Euler-Bernoulli theory. Therefore, we expect the *w–a* relation (3.13), which we derived using Woinowsky-Krieger theory, to reduce to the *w–a* relation (2.7), which was derived by Mastrangelo and Hsu [29] using Euler-Bernoulli theory. We find that this is in fact the case. For example, if we expand $\langle \hat{\Pi}_{\mathcal{E}} \rangle$ given by (3.12) in powers of $\hat{g}$ about $\hat{g} = 0$ in the *w–a* relation (3.13), the relation attains the aymptotic form

$$\hat{w} = \frac{3\hat{g}^2}{2\hat{a}^4} + o(\hat{g}^2), \quad \text{as } \hat{g} \to 0. \tag{4.10}$$

In terms of non-dimensional variables the *w–a* relation (2.7) reads as

$$\hat{w} = \frac{3\hat{g}^2}{2\hat{a}^4}. \tag{4.11}$$

As can be noted from (4.10) and (4.11), the *w–a* relation (3.13) and the *w–a* relation (2.7) are the same up to $o(\hat{g}^2)$ terms.

Interestingly, the *w–a* relation (2.9) derived by Mastrengelo and Hus [28] using a nonlinear beam theory does not match the Euler-Bernoulli *w–a* relation (2.7) in the limit $\hat{g} \to 0$. On writing the *w–a* relation (2.9) in terms of non-dimensional variables and expanding the right hand side in powers of $\hat{g}$ about $\hat{g} = 0$, it attains the asymptotic form

$$\hat{w} = \frac{8\hat{g}^2}{5\hat{a}^4} + o(\hat{g}^2). \tag{4.12}$$

Note that the numerical factor in the leading order term in (4.12) is $8/5$. Whereas, if the *w–a* relation (2.9) were to match the *w–a* relation (2.7) exactly in the limit $\hat{g} \to 0$ then this numerical factor should have been $3/2$. In summary, our results for the *w–a* relation are consistent with Euler-Bernoulli theory in the limit $\hat{g} \to 0$, while those given by Mastrangelo and Hsu [56] are not.

5. Conclusion

We believe that the flexibility of a vibration-based method allows it to be applied to a wider variety of problems. Beyond the reliability of MEMS, the topic of adhesion at submicron scales is important in its own right. For example, some of the unique capabilities of biological materials, such as insect wings [66] and the adhesive toe pads of geckos [67], are thought to arise through adhesion at small scales. In addition, the adhesion between solids is generally measured using axisymmetric, contact mechanics based methods [68]. However, surface roughness is known to cause considerable difficulties in unambiguously measuring w using such methods [69, 70, 71]. Therefore, it would be interesting to see how competitive the proposed vibration based method for measuring w would be in comparison to the contact mechanics based methods.

Implicit in our and previous models of the adhered microbeam is the assumption that the interbody adhesion forces are infinitesimally short ranged. This is similar to what is assumed in, for example, the Johnson-Kendall-Roberts (JKR) adhesive contact model [72]. Equation (2.3), which states that $\Pi_s = red - w(L-a)W$, is a consequence of this assumption. However, studies have shown that adhesive forces (which, at submicron scales, are primarily due to van der Waals interactions [73]) can act over long distances [74] and have been measured to act over distances as large as a micrometer [75]. Therefore, the forces on the adhered microbeam can act over its full length and are spatially non-uniform. It remains to be seen how important of an effect such non-uniformity has and if the assumption of the interbody adhesion forces being infinitesimally short ranged is an acceptable approximation. We plan to explore this effect in future experiments.

Reference

[1] J. Bryzek, Impact of mems technology on society, Sensors and Actuators A: Physical 56 (1-2) (1996) 1–9.

[2] J. W. Judy, Microelectromechanical systems (mems): fabrication, design and applications, Smart materials and Structures 10 (6) (2001) 1115.

[3] A. Nisar, N. Afzulpurkar, B. Mahaisavariya, A. Tuantranont, Mems-based micropumps in drug delivery and biomedical applications, Sensors and Actuators B: Chemical 130 (2) (2008) 917–942.

[4] A. Neukermans, R. Ramaswami, Mems technology for optical networking applications, IEEE Communications Magazine 39 (1) (2001) 62–69.

[5] G. M. Rebeiz, J. B. Muldavin, Rf mems switches and switch circuits, IEEE Microwave magazine 2 (4) (2001) 59–71.

[6] I. De Wolf, W. M. van Spengen, Techniques to study the reliability of metal RF MEMS capacitive switches, Microelectronics reliability 42 (9-11) (2002) 1789–1794.

[7] W. M. Van Spengen, R. Puers, I. De Wolf, A physical model to predict stiction in MEMS, Journal of micromechanics and microengineering 12 (5) (2002) 702.

[8] R. Maboudian, Adhesion and friction issues associated with reliable operation of MEMS, MRS Bulletin 23 (06) (1998) 47–51.

[9] H. Guckel, J. J. Sniegowski, T. R. Christenson, S. Mohney, T. F. Kelly, Fabrication of micromechanical devices from polysilicon films with smooth surfaces, Sensors and Actuators 20 (1-2) (1989) 117–122.

[10] R. Maboudian, R. T. Howe, Critical review: adhesion in surface micromechanical structures, Journal of Vacuum Science & Technology B 15 (1) (1997) 1–20.

[11] N. Tas, T. Sonnenberg, H. Jansen, R. Legtenberg, M. Elwenspoek, Stiction in surface micromachining, Journal of Micromechanics and Microengineering 6 (4) (1996) 385.

[12] Y. Fukuta, H. Fujita, H. Toshiyoshi, Vapor hydrofluoric acid sacrificial release technique for micro electro mechanical systems using labware, Japanese Journal of Applied Physics 42 (6R) (2003) 3690.

[13] G. T. Mulhern, D. S. Soane, R. T. Howe, Supercritical carbon dioxide drying of microstructures, in: Proc. 7th Int. Conf. Solid-State Sensors and Actuators (Transducers' 93), 1993, pp. 7–10.

[14] S. D. Senturia, Microsystem design, Springer Science & Business Media, 2007.

[15] W. M. Van Spengen, R. Puers, I. De Wolf, The prediction of stiction failures in MEMS, IEEE Transactions on Device and Materials reliability 3 (4) (2003) 167–172.

[16] B. P. Gogoi, C. H. Mastrangelo, Adhesion release and yield enhancement of microstructures using pulsed lorentz forces, Journal of Microelectromechanical Systems 4 (4) (1995) 185–192.

[17] L.-S. Fan, Y.-C. Tai, R. S. Muller, IC-processed electrostatic micromotors, Sensors and actuators 20 (1) (1989) 41–47.

[18] A. A. Savkar, K. D. Murphy, Using periodic electrical excitation to achieve stick-release in micro-cantilevers, in: MOEMS-MEMS 2006 Micro and Nanofabrication, International Society for Optics and Photonics, 2006, pp. 611102–611102.

[19] A. A. Savkar, K. D. Murphy, Z. C. Leseman, T. J. Mackin, M. R. Begley, On the use of structural vibrations to release stiction failed MEMS, Journal of Microelectromechanical Systems 16 (1) (2007) 163–173.

[20] A. A. Savkar, K. D. Murphy, Mechanics of the dynamic release process for stiction failed microcantilever beams using structural vibrations, in: MOEMS-MEMS 2008 Micro and Nanofabrication, International Society for Optics and Photonics, 2008, pp. 68840A–68840A.

[21] R. L. Alley, P. Mai, K. Komvopoulos, R. T. Howe, Surface roughness modification of interfacial contacts in polysilicon microstructures, in: Transducers, Vol. 93, 1993, pp. 288–291.

[22] M. R. Houston, R. Maboudian, R. T. Howe, Ammonium fluoride antistiction treatments for polysilicon microstructures, in: Solid-State Sensors and Actuators, 1995 and Eurosensors IX.. Transducers' 95. The 8th International Conference on, Vol. 1, IEEE, 1995, pp. 210–213.

[23] U. Srinivasan, M. R. Houston, R. T. Howe, R. Maboudian, Alkyltrichlorosilane-based self-assembled monolayer films for stiction reduction in silicon micromachines, Journal of Microelectromechanical Systems 7 (2) (1998) 252–260.

[24] M. R. Houston, R. T. Howe, R. Maboudian, Effect of hydrogen termination on the work of adhesion between rough polycrystalline silicon surfaces, Journal of Applied Physics 81 (8) (1997) 3474–3483.

[25] M. W. Lane, J. M. Snodgrass, R. H. Dauskardt, Environmental effects on interfacial adhesion, Microelectronics Reliability 41 (9-10) (2001) 1615–1624.

[26] D. Maugis, Elements of surface physics, in: Contact, Adhesion and Rupture of Elastic Solids, Springer, 2000, pp. 1–79.

[27] K. Kendall, The adhesion and surface energy of elastic solids, Journal of Physics D: Applied Physics 4 (8) (1971) 1186.

[28] C. H. Mastrangelo, C. H. Hsu, Mechanical stability and adhesion of microstructures under capillary forces. II. experiments, Journal of Microelectromechanical Systems 2 (1) (1993) 44–55.

[29] C. H. Mastrangelo, C. H. Hsu, A simple experimental technique for the measurement of the work of adhesion of microstructures, in: Solid-State Sensor and Actuator Workshop, 1992. 5th Technical Digest., IEEE, IEEE, 1992, pp. 208–212.

[30] M. P. De Boer, T. A. Michalske, Accurate method for determining adhesion of cantilever beams, Journal of applied physics 86 (2) (1999) 817–827.

[31] R. M. Langdon, Resonator sensors—a review, Journal of Physics E: Scientific Instruments 18 (2) (1985) 103.

[32] J. W. Gardner, V. K. Varadan, O. O. Awadelkarim, Microsensors, MEMS, and smart devices, Vol. 1, Wiley Online Library, 2001.

[33] Nanoworld, Special application cantilevers (2017).
URL http://www.nanoworld.com/tipless-afm-tip-arrow-tl1

[34] M. Suter, O. Ergeneman, J. Zürcher, S. Schmid, A. Camenzind, B. Nelson, C. Hierold, Superparamagnetic photocurable nanocomposite for the fabrication of microcantilevers, Journal of Micromechanics and Microengineering 21 (2) (2011) 025023.

[35] J. L. Hutter, J. Bechhoefer, Calibration of atomic-force microscope tips, Review of Scientific Instruments 64 (7) (1993) 1868–1873.

[36] J. E. Sader, I. Larson, P. Mulvaney, L. R. White, Method for the calibration of atomic force microscope cantilevers, Review of Scientific Instruments 66 (7) (1995) 3789–3798.

[37] J. E. Sader, J. W. Chon, P. Mulvaney, Calibration of rectangular atomic force microscope cantilevers, Review of Scientific Instruments 70 (10) (1999) 3967–3969.

[38] R. Levy, M. Maaloum, Measuring the spring constant of atomic force microscope cantilevers: thermal fluctuations and other methods, Nanotechnology 13 (1) (2001) 33.

[39] N. Burnham, X. Chen, C. Hodges, G. Matei, E. Thoreson, C. Roberts, M. Davies, S. Tendler, Comparison of calibration methods for atomic-force microscopy cantilevers, Nanotechnology 14 (1) (2002) 1.

[40] M. A. Monn, H. Kesari, Enhanced bending failure strain in biological glass fibers due to internal lamellar architecture, Journal of the Mechanical Behavior of Biomedical MaterialsIn press.

[41] H. Elettro, S. Neukirch, A. Antkowiak, F. Vollrath, Adhesion of dry and wet electrostatic capture silk of uloborid spider, Naturwissenschaften 102 (7-8) (2015) 41.

[42] K. F. Graff, Wave motion in elastic solids, Courier Corporation, 2012.

[43] D. J. Ijntema, H. A. Tilmans, Static and dynamic aspects of an air-gap capacitor, Sensors and Actuators A: Physical 35 (2) (1992) 121–128.

[44] H. A. Tilmans, M. Elwenspoek, J. H. Fluitman, Micro resonant force gauges, Sensors and Actuators A: Physical 30 (1-2) (1992) 35–53.

[45] H. A. Tilmans, R. Legtenberg, Electrostatically driven vacuum-encapsulated polysilicon resonators: Part II. theory and performance, Sensors and Actuators A: Physical 45 (1) (1994) 67–84.

[46] M. H. Ghayesh, H. Farokhi, M. Amabili, Nonlinear behaviour of electrically actuated MEMS resonators, International Journal of Engineering Science 71 (Supplement C) (2013) 137–155. doi:10.1016/j.ijengsci.2013.05.006.

[47] M. H. Ghayesh, M. Amabili, H. Farokhi, Nonlinear forced vibrations of a microbeam based on the strain gradient elasticity theory, International Journal of Engineering Science 63 (Supplement C) (2013) 52–60. doi:10.1016/j.ijengsci.2012.12.001.

[48] M. H. Ghayesh, H. Farokhi, M. Amabili, In-plane and out-of-plane motion characteristics of microbeams with modal interactions, Composites Part B: Engineering 60 (Supplement C) (2014) 423–439. doi:10.1016/j.compositesb.2013.12.074.

[49] M. H. Ghayesh, H. Farokhi, M. Amabili, Nonlinear dynamics of a microscale beam based on the modified couple stress theory, Composites Part B: Engineering 50 (Supplement C) (2013) 318–324. doi:10.1016/j.compositesb.2013.02.021.

[50] M. H. Ghayesh, H. Farokhi, G. Alici, Size-dependent performance of microgyroscopes, International Journal of Engineering Science 100 (Supplement C) (2016) 99–111. doi:10.1016/j.ijengsci.2015.11.003.

[51] M. H. Ghayesh, M. Amabili, H. Farokhi, Three-dimensional nonlinear size-dependent behaviour of Timoshenko microbeams, International Journal of Engineering Science 71 (Supplement C) (2013) 1–14. doi:10.1016/j.ijengsci.2013.04.003.

[52] H. Farokhi, M. H. Ghayesh, S. Hussain, Large-amplitude dynamical behaviour of microcantilevers, International Journal of Engineering Science 106 (Supplement C) (2016) 29–41. doi:10.1016/j.ijengsci.2016.03.002.

[53] H. Farokhi, M. H. Ghayesh, Nonlinear resonant response of imperfect extensible Timoshenko microbeams, International Journal of Mechanics and Materials in Design 13 (1) (2017) 43–55. doi:10.1007/s10999-015-9316-z.

[54] Y. Zhang, Y.-P. Zhao, Vibration of an adhered microbeam under a periodically shaking electrical force, Journal of Adhesion Science and Technology 19 (9) (2005) 799–815.

[55] S. Woinowsky-Krieger, The effect of axial force on the vibration of hinged bars, Journal of Applied Mechanics 17 (1950) 35–36.

[56] C. H. Mastrangelo, C. H. Hsu, Mechanical stability and adhesion of microstructures under capillary forces. I. basic theory, Journal of Microelectromechanical systems 2 (1) (1993) 33–43.

[57] H. Espinosa, Y. Zhu, M. Fischer, J. Hutchinson, An experimental/computational approach to identify moduli and residual stress in mems radio-frequency switches, Experimental Mechanics 43 (3) (2003) 309–316.

[58] M. P. De Boer, J. A. Knapp, T. M. Mayer, T. A. Michalske, Role of interfacial properties on MEMS performance and reliability, in: Industrial Lasers and Inspection (EUROPTO Series), International Society for Optics and Photonics, 1999, pp. 2–15.

[59] R. Legtenberg, H. A. Tilmans, J. Elders, M. Elwenspoek, Stiction of surface micromachined structures after rinsing and drying: model and investigation of adhesion mechanisms, Sensors and actuators A: Physical 43 (1) (1994) 230–238.

[60] A. A. Griffith, The phenomena of rupture and flow in solids, Philosophical transactions of the royal society of london. Series A, containing papers of a mathematical or physical character 221 (1921) 163–198.

[61] M. E. Gurtin, Configurational forces as basic concepts of continuum physics, Vol. 137, Springer Science & Business Media, 2008.

[62] D. Maugis, Study of some geometries, in: Contact, Adhesion and Rupture of Elastic Solids, Springer, 2000, pp. 345–401.

[63] A. H. Nayfeh, P. F. Pai, Linear and nonlinear structural mechanics, John Wiley & Sons, 2008.

[64] C. L. Dym, I. H. Shames, Dynamics of beams and plates, in: Solid Mechanics, Springer, 2013, pp. 373–447.

[65] T. Belytschko, W. K. Liu, B. Moran, K. Elkhodary, Nonlinear finite elements for continua and structures, John wiley & sons, 2013.

[66] G. S. Watson, J. A. Watson, S. Hu, C. L. Brown, B. Cribb, S. Myhra, Micro and nanostructures found on insect wings–designs for minimising adhesion and friction, International Journal of Nanomanufacturing 5 (1-2) (2009) 112–128.

[67] K. Autumn, P. H. Niewiarowski, J. B. Puthoff, Gecko adhesion as a model system for integrative biology, interdisciplinary science, and bioinspired engineering, Annual Review of Ecology, Evolution, and Systematics 45 (2014) 445–470.

[68] K. R. Shull, Contact mechanics and the adhesion of soft solids, Materials Science and Engineering: R: Reports 36 (1) (2002) 1–45.

[69] H. Kesari, A. J. Lew, Effective macroscopic adhesive contact behavior induced by small surface roughness, Journal of the Mechanics and Physics of Solids 59 (12) (2011) 2488–2510.

[70] H. Kesari, J. C. Doll, B. L. Pruitt, W. Cai, A. J. Lew, Role of surface roughness in hysteresis during adhesive elastic contact, Philosophical Magazine & Philosophical Magazine Letters 90 (12) (2010) 891–902.

[71] W. Deng, H. Kesari, Molecular statics study of depth-dependent hysteresis in nano-scale adhesive elastic contacts, Modelling and Simulation in Materials Science and Engineering 25 (5) (2017) 055002.

[72] K. Johnson, K. Kendall, A. Roberts, Surface energy and the contact of elastic solids, in: Proceedings of the Royal Society of London A: Mathematical, Physical and Engineering Sciences, Vol. 324, The Royal Society, 1971, pp. 301–313.

[73] F. W. DelRio, M. P. de Boer, J. A. Knapp, E. D. Reedy, P. J. Clews, M. L. Dunn, The role of van der waals forces in adhesion of micromachined surfaces, Nature materials 4 (8) (2005) 629.

[74] H. Casimir, D. Polder, The influence of retardation on the london-van der waals forces, Physical Review 73 (4) (1948) 360.

[75] J. Kitchener, A. Prosser, Direct measurement of the long-range van der waals forces 242 (1230) (1957) 403–409.

Appendix A. Derivation of (3.10)

red We arrive at (3.10) through approximating the adhered beam's static displacements using the solution given by Mastrangelo and Hsu [29], which is based on Euler-Bernoulli beam theory. Specifically, using (2.5) and the fact that longitudinal displacements are assumed to be of negligible magnitude in the Euler-Bernoulli theory, we approximate ζ_0 and η_0 as

$$\zeta_0(\xi) \approx 0, \tag{A.1}$$

$$\eta_0(\xi) \approx \hat{g}\xi^2(2\xi - 3). \tag{A.2}$$

We use these approximations of ζ_0 and η_0 to approximate ϵ_0^2, which was previously defined in Section 3 as

$$\epsilon_0^2 := 3\hat{a}\frac{d\zeta_0}{d\xi} + \frac{3}{2}\left(\frac{\partial\eta_0}{\partial\xi}\right)^2. \tag{A.3}$$

Substituting the approximations (A.1) and (A.2) into (A.3), we get that ϵ_0^2 is approximately equal to

$$\frac{9\hat{g}^2}{5}. \tag{A.4}$$

However, we found the expression (A.4) to be a poor approximation of ϵ_0. To obtain a better approximation for the dependence of ϵ_0 on $\hat{g}$, we compute new approximations for ζ_0 and η_0 by solving equations (3.6a)–(3.7b) under the assumption that ϵ_0^2 in them is given by (A.4). Then, we substitute the newly obtained approximations for ζ_0 and η_0 into (A.3) to finally arrive at (3.10).